

Levulinic Acid Production from Waste Corncob Biomass Using an Environmentally Benign WO_3 -Grafted $\text{ZnCo}_2\text{O}_4@/\text{CeO}_2$ Bifunctional Heterogeneous Catalyst

Fouzia Perveen,* Muhammad Farooq,* Anita Ramli, Abdul Naeem, Ihtisham Wali khan, Tooba Saeed, and Jehangeer khan

Cite This: *ACS Omega* 2023, 8, 333–345

Read Online

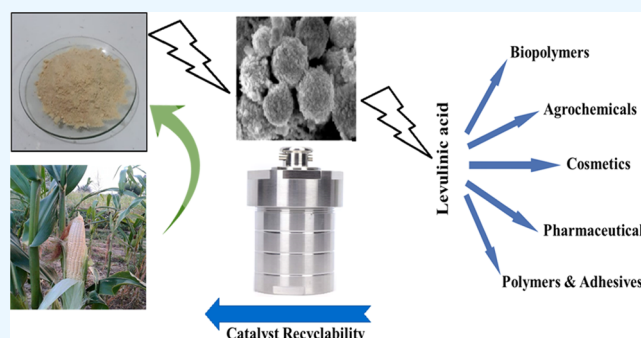
ACCESS |

Metrics & More

Article Recommendations

Supporting Information

ABSTRACT: Herein, a novel and environmentally benign solid catalyst was fabricated by grafting WO_3 active species onto the $\text{ZnCo}_2\text{O}_4@/\text{CeO}_2$ support for efficient levulinic acid production from corncob waste biomass. The morphological, compositional, and textural properties of the designed catalyst were investigated using different characterization techniques to identify suitable catalyst formulation with enhanced catalytic activity and stability. The results demonstrated that WO_3 active species were successfully loaded with uniform distribution onto the support to develop a robust catalyst with both acidic and basic sites. The experimental investigation showed that among the catalysts, $\text{WO}_3(10 \text{ wt } \%) / \text{ZnCo}_2\text{O}_4@/\text{CeO}_2$ exhibited the best catalytic activity, providing a maximum levulinic acid yield of 78.49% at the optimal conditions of 6 wt % catalyst dosage, reaction temperature of 180 °C, and reaction time of 200 min. The presence of an optimum number of both acid and base active sites on the catalyst surface could lead to the highest catalytic activity of the synthesized catalyst. Finally, the reusability investigation indicated that the synthesized catalyst possessed sufficient recyclability of up to four times for the levulinic acid production from the selected biomass with negligible drop in the catalytic activity.



1. INTRODUCTION

Recently, global demand for energy and chemicals has increased alarmingly due to rapid increase in population growth and industrialization.¹ Moreover, fossil fuels have remained the main source of driving social and industrial progress from ancient times. However, reliance on fossil fuels will not sustain the global energy demand in the long run due to their limited resources on the earth. The environmental pollution related to fossil fuel combustion has further endangered the sustainability of the planet.² Consequently, the researchers have realized that the shift toward renewable sources is imperative for sustainable growth.^{3,4}

Research into utilizing waste biomass has attracted great attention all over the world to produce different biobased products and sustainable energy infrastructure.^{5,6} Lignocellulosic biomass consists of mainly three parts: lignin, hemicellulose, and cellulose.^{7,8} However, the biomass composition may vary with the source and area. Typically, biomass consists of 75% carbohydrates in the form of hemicelluloses and celluloses, consisting primarily of C_5 and C_6 sugars, respectively.^{9,10} It has been noted that among the biomass components, cellulose and hemicellulose can more easily be converted into useful chemical components as compared to lignin.¹¹

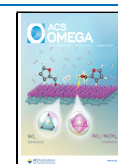
Lignocellulosic biomass mainly comes either from agricultural residues (such as bagasse, wheat straw, corncob, rice husk) or forestry wastes.¹² Pakistan is an agriculture-based country and is bestowed with sufficient biomass residues. Unfortunately, these biomass wastes are not utilized properly, causing a wastage of resources as well as environmental pollution. Therefore, proper utilization of the available biomass resources is crucial for the sustainable development and growth of society.

Corncob is cultivated in different areas of Pakistan over an area of approximately 0.9 Mha, with an annual grain production of 1.3 million tons.¹³ Corncob (byproduct of corn grains) is discarded either as waste or burnt for domestic cooking purposes, causing serious environmental damage. In this context, the researchers strongly recommend utilizing such type of waste biomass as a raw material for biofuel production

Received: July 19, 2022

Accepted: November 10, 2022

Published: December 23, 2022



and platform chemicals to boost the economy and mitigate environmental issues in a justifiable way.¹⁴

Lignocellulosic biomass can be converted into biofuels and platform chemicals (levulinic acid, hydroxymethylfurfural, formic acid, and furfural) using different technologies such as combustion, gasification, pyrolysis, fermentation processes, and enzymatic hydrolysis routes.^{8,15,16} Levulinic acid has been identified as a promising building block and energy-rich platform chemical, finding a large number of applications in pharmaceuticals, food industries, fragrances, fuel industries, and resins.^{17–21}

Conventionally, levulinic acid is prepared at elevated temperatures (100–250 °C) from C6 sugars of the biomass using homogeneous acid-catalyzed hydrolysis.²² But these homogeneous catalyzed levulinic acid production processes pose several disadvantages like recycling, product separation, high toxicity, reactor corrosion, and environmental pollution.^{23,24}

Therefore, researchers encourage the use of solid acid catalysts for sustainable levulinic acid production and avoid the problems associated with homogeneous acid-catalyzed biomass hydrolysis. The solid acid catalysts are environmentally benign, less corrosive, and safe to handle and possess easy separation and recycling characteristics with improved catalytic activity in levulinic acid production from biomass.²⁵ However, there is still room for improvement to develop a more robust catalyst with enhanced catalytic activity and stability for sustainable levulinic acid production from biomass.

The main objective of this research work is to design an efficient catalyst by grafting WO₃ onto the ZnCo₂O₄@CeO₂ support with both acidic and basic sites for sustainable production of Levulinic acid from selected corncob biomass. To achieve the aforementioned objective, first the ZnCo₂O₄ support was synthesized by partially substituting Co₃O₄ with zinc metal to introduce the desired physicochemical properties such as good monodispersity, rich redox reactions, and acid–base bifunctionality. The ZnCo₂O₄ particles were further coated with CeO₂ to form hybrids, i.e., ZnCo₂O₄@CeO₂ microspheres with improved physicochemical properties such as high thermal stability, acid–base bifunctionality, etc.

Various acid precursors such as SO₃H,²⁶ TPA,²⁷ MoO₃,²⁸ and WO₃²⁹ have been used to develop a heterogeneous catalyst for different applications. However, among them, the WO₃ acid precursor has been identified as a promising active species to develop a robust heterogeneous catalyst due to its numerous advantages such as high chemical stability, low toxicity, low cost, great abundance, and high recyclability.³⁰ Moreover, the important physicochemical properties were also investigated to identify a suitable catalyst formulation.

2. EXPERIMENTAL SECTION

2.1. Reagents. All of the reagents such as ethanol (Sigma-Aldrich), acetone (Sigma-Aldrich), sulfuric acid (Scharlau), benzene (Scharlau), sodium hydroxide (Scharlau), zinc acetate (Daejung), cobalt acetate (Daejung), ethylene glycol (Daejung), cerium nitrate (Daejung), hexamethylenetetramine (Daejung), ammonium molybdate (Daejung), and ammonium tungstophosphoric acid (Scharlau) employed in the current work were of high purity and utilized without any prior treatment.

2.2. Feedstock Collection. In this study, corncob biomass was employed as a feedstock for levulinic acid production. Corncob biomass waste was collected from the University of

Peshawar, Khyber Pakhtunkhwa, Pakistan. The collected biomass was first washed and later sun-dried. The corncob was ground to fine powder and sieved. The important components (extractive, hemicellulose, cellulose, and lignin) of the biomass were estimated by established methods.³¹

2.3. Catalyst Preparation. **2.3.1. Synthesis of ZnCo₂O₄ Microspheres.** The ZnCo₂O₄ microspheres were first synthesized by a hydrothermal method. Typically, 0.22 g of Zn(CH₃COO)₂·2H₂O and 0.50 g of Co(CH₃COO)₂·4H₂O were dissolved in 50 mL of ethylene glycol at 50 °C for 30 min to synthesize ZnCo₂O₄ with a Zn-to-Co metal ratio of 1:2. The reaction mixture was then poured into an autoclave and kept in an oven at 170 °C for 2 h. After completion of the reaction, the autoclave was cooled naturally. The particles thus obtained were centrifuged and washed with acetone and ethanol, followed by vacuum drying at 60 °C for 12 h. Lastly, the ZnCo-glycolate sample was calcined at 500 °C for 5 h by thermogravimetric analysis to obtain ZnCo₂O₄ microspheres.

2.3.2. Synthesis of ZnCo₂O₄@CeO₂ Microspheres. The required amount of ZnCo₂O₄ microspheres was first ultrasonically scattered in 80 mL of water/ethanol (1:1 v/v) solution. About 0.021 g of Ce(NO₃)₃ and 0.014 g of hexamethylenetetramine (HMT) were dissolved in separate beakers to prepare transparent solutions. Later, the above salt solutions were mixed together and then added to the already dispersed ZnCo₂O₄ particles with vigorous stirring. The mixture was then transferred into an autoclave and heated at 60 °C for 2 h. After completion of the reaction, the autoclave was cooled, and the black precipitate was collected using a centrifuge. The synthesized particles were further purified by washing with distilled water and ethanol and vacuum-dried at 60 °C for 12 h. Later, the sample was thermally treated at 500 °C in a muffle furnace by TGA analysis to obtain the ZnCo₂O₄@CeO₂ support.

2.3.3. Modification of the ZnCo₂O₄@CeO₂ Support with WO₃ Active Species. WO₃ active species were grafted onto the ZnCo₂O₄@CeO₂ support by an impregnation method.³² Typically, 0.3 g of the synthesized support was dispersed in an aqueous solution of (NH₄)₆ H₂W₁₂O₄₀·xH₂O (ammonium tungstophosphoric acid) with constant stirring to achieve 5 wt % WO₃ loading. The above mixture was dried carefully. The synthesized catalyst was activated thermally at 400 °C for 5 h in accordance with the TGA results. The WO₃/ZnCo₂O₄@CeO₂ catalyst with 5 wt % WO₃ loading was stored properly for experimental investigations. The catalysts with 10 and 15 wt % WO₃ loading were also prepared by a similar procedure.

2.4. Catalyst Characterization. The thermal degradation behavior of the synthesized catalyst was investigated with a thermal gravimetric analyzer (PerkinElmer) in a N₂ atmosphere. N₂ adsorption–desorption analysis was carried out on a Micromeritics TriStar II 3020 (V1.04) to study the textural properties of the catalyst. The XRD analysis (Bruker AXS D8 Advance Diffractometer) was conducted to study the crystallinity of the catalyst. The morphological behavior and elemental composition of the catalyst were determined by FESEM (Zeiss SUPRA 55-VP). The basicity and acidity characteristics of the catalyst were investigated by CO₂-TPD and NH₃-TPD analysis, respectively (Thermo Scientific TPDRO 1100).

2.5. Catalytic Performance Procedure. The performance of the designed catalyst in the production of levulinic acid from selected corncob biomass was investigated in a stainless steel reactor under predetermined reaction conditions of 4 wt

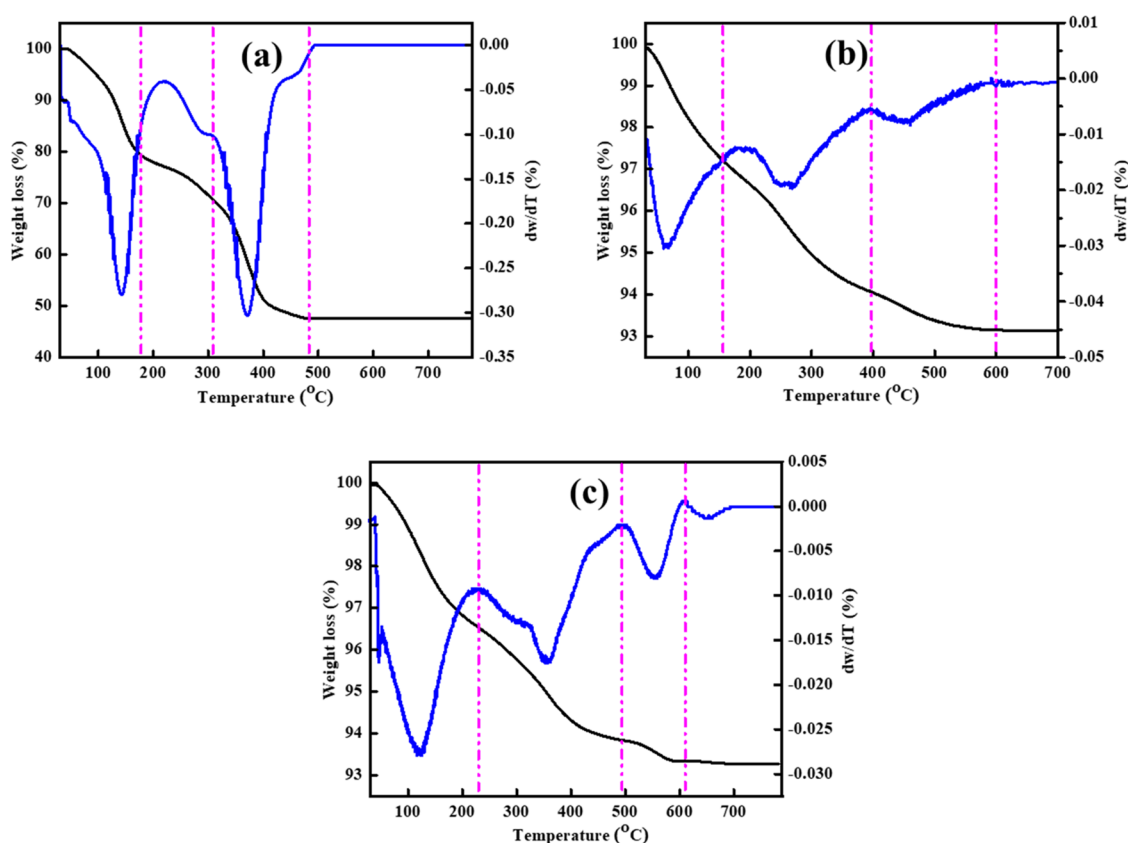


Figure 1. TG-DTA curves for (a) ZnCo_2O_4 microspheres, (b) $\text{ZnCo}_2\text{O}_4@ \text{CeO}_2$ catalyst, and (c) WO_3 -modified $\text{ZnCo}_2\text{O}_4@ \text{CeO}_2$ catalyst.

% catalyst dosage, a reaction temperature of 180 °C, and a reaction time of 200 min. In a typical experiment, about 5 g of finely ground particles of corncob biomass and 4 wt % $\text{WO}_3/\text{ZnCo}_2\text{O}_4@ \text{CeO}_2$ catalyst were dispersed in 100 mL of distilled water. The mixture was later transferred to a stainless steel reactor and heated up to 180 °C for 200 min in an oven. After the reaction completion, the reaction mixture was filtered to collect the catalyst, and the liquid portion was stored for further investigation. Moreover, the reusability of the synthesized catalyst was also evaluated for levulinic acid production from selected corncob biomass to investigate its economic viability for large-scale production.

2.6. Product Analysis. The liquid portion of the reaction mixture was extracted three times with 1% (v/v) ethyl acetate and then transferred into a centrifuge tube. This solution was then centrifuged at 2000 rpm for 5 min. This resulted in the formation of two layers: an aqueous phase (bottom layer) and an organic phase (upper layer). The organic phase from the upper layer was withdrawn and then dried at 50 °C for 30 min in a rotary evaporator to remove the moisture content. The resultant liquid portion was further diluted with ethyl acetate and analyzed by gas chromatography (Thermo Scientific GC Focus Series DSQ, Instrument Software Version: 2.0.7) for levulinic acid identification. The various components of the sample were identified by comparing with the GCMS library. Moreover, the levulinic acid yield was estimated using the following equation^{33–35}

$$\text{LA yield (\%)} = \frac{\text{amount of LA}}{\text{initial biomass loading}} \times 100\% \quad (1)$$

2.7. Results Reproducibility. The results reproducibility for the production of levulinic acid from corncob biomass was investigated by carrying out each experiment three times in the stainless steel autoclave reactor and high-pressure reactor (model: THR-100, Toption Group Co., Limited). The standard error was estimated from the obtained results and represented by an error bar to define the economic viability of the levulinic acid production from corncob biomass using the designed catalyst.

3. RESULTS AND DISCUSSION

3.1. Catalyst Characterization. **3.1.1. Thermal Gravitimetric Analysis (TGA).** The thermal degradation behavior of the designed catalyst was studied by thermogravimetric analysis (Figure 1). The TG/DTA curves of the ZnCo_2O_4 particles showed a maximum weight loss of 20.14% in the 30–168 °C temperature range. This endothermic peak is related to the removal of water adsorbed physically. The endothermic peak that appeared in the 168–400 °C range is related to the evaporation of chemically bonded water and decomposition of the ZnCo_2O_4 glycolate sample. Moreover, a small weight loss of 4.4% also occurred over the 400 and 480 °C temperature range, which can be assigned to the decomposition of some intermediate particles. Further, it was observed that beyond 500 °C, no weight loss occurred, indicating that the process of decomposition has been completed. In view of the above, ZnCo_2O_4 glycolate particles were prepared in the muffle furnace at 500 °C at a treatment time of 5 h.

However, when ZnCo_2O_4 core particles were modified with the CeO_2 precursor, the thermal degradation behavior was slightly different from that of the ZnCo_2O_4 sample. The weight loss of 3.12% was noticed at a lower temperature of 30–181

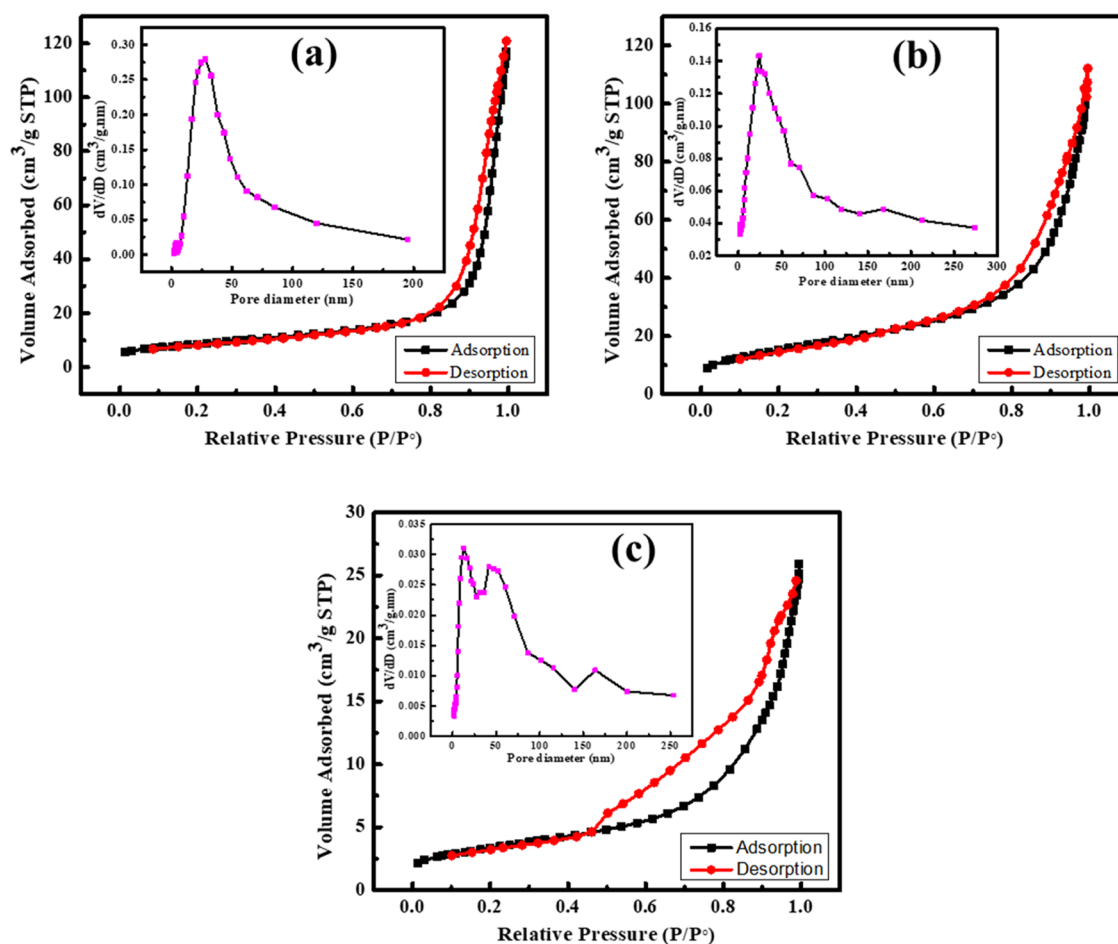


Figure 2. N_2 adsorption–desorption isotherm of (a) $ZnCo_2O_4$ microspheres, (b) $ZnCo_2O_4@CeO_2$ catalyst, and (c) WO_3 -modified $ZnCo_2O_4@CeO_2$ catalyst.

$^{\circ}C$, which is generally related to the evaporation of loosely bonded water molecules present in the sample. The second weight loss of 2.76% that appeared in the temperature range of 181–390 $^{\circ}C$ is related to the removal of chemically bonded water molecules and decomposition of nitrate molecules in the sample.³⁶ Similarly, a small peak with a weight loss of 0.94% was also noticed at higher temperatures (390 and 600 $^{\circ}C$), which might be due to the decomposition of remaining $Ce(NO_3)_2 \cdot 6H_2O$ molecules in the sample.³⁷ Further, it was noticed that beyond 600 $^{\circ}C$, no weight loss was recorded, indicating that the decomposition of the sample has been completed. In light of thermogravimetric analysis, the $ZnCo_2O_4@CeO_2$ support was prepared at 600 $^{\circ}C$ in a muffle furnace for 5 h. This has also been discussed in detail in our previous manuscript.³⁸

The thermal degradation behavior of the uncalcined $WO_3/ZnCo_2O_4@CeO_2$ catalyst was also determined, as shown in Figure 1c. It can be seen that the catalyst shows thermal degradation in several stages. The TGA thermogram showed a 3.09% weight loss at lower temperatures in the range of 30–194 $^{\circ}C$, corresponding to the removal of physically and chemically adsorbed water from the sample.³⁹ The weight loss of 2.99% that appeared in the temperature range of 194–460 $^{\circ}C$ is attributed to the decomposition of WO_3 precursor molecules.⁴⁰ Similarly, a small weight loss of 0.57% also appeared at higher temperatures in the range of 460–590 $^{\circ}C$, which can be attributed to the decomposition of remaining

precursor molecules. The TGA thermogram further illustrates that the sample becomes stable beyond 700 $^{\circ}C$, indicating that this temperature is suitable for the thermal activation of the catalyst.

3.1.2. N_2 Adsorption–Desorption Analysis (BET). The textural properties of the different catalysts were studied by the N_2 adsorption–desorption technique, as shown in Figure 2 and tabulated in Table 1. It can be seen that all of the isotherms justify type IV isotherm with well-developed H2 hysteresis loops and hence confirm that the sample is mesoporous in nature.⁴¹

The BJH pore size of the $ZnCo_2O_4@CeO_2$ support was recorded to be decreased as compared to $ZnCo_2O_4$ bare particles, indicating that the CeO_2 moieties have deposited within the channels of the $ZnCo_2O_4$ particles. In contrast, the

Table 1. Textural Properties of Bare $ZnCo_2O_4$ Spheroids, $ZnCo_2O_4@CeO_2$ Catalyst, and WO_3 -Modified $ZnCo_2O_4@CeO_2$ Catalyst

catalyst	textural properties		
	BET surface area, S_A (m^2/g)	pore volume, V_p (cm^3/g)	pore diameter, D_p (nm)
$ZnCo_2O_4$	40.58	0.19	22.64
$ZnCo_2O_4@CeO_2$	62.38	0.18	11.72
$WO_3/ZnCo_2O_4@CeO_2$	36.36	0.04	10.27

surface area of the $\text{ZnCo}_2\text{O}_4@\text{CeO}_2$ support was recorded to be slightly higher ($62.38 \text{ m}^2/\text{g}$) as compared to the bare ZnCo_2O_4 particles, indicating that the growth of small CeO_2 particles was dispersed on the ZnCo_2O_4 matrix as also discussed previously.³⁸

The surface area of the support sufficiently decreased when WO_3 active species were grafted to achieve the $\text{WO}_3/\text{ZnCo}_2\text{O}_4@\text{CeO}_2$ catalyst. The decrease in the surface area might be due to the blockage of the pores when WO_3 active species were impregnated onto the support.

3.1.3. X-ray Diffraction Analysis (XRD). The XRD spectra of bare ZnCo_2O_4 spheroids, $\text{ZnCo}_2\text{O}_4@\text{CeO}_2$ support, and WO_3 -modified $\text{ZnCo}_2\text{O}_4@\text{CeO}_2$ catalyst are depicted in Figure 3. The XRD results of the synthesized ZnCo_2O_4

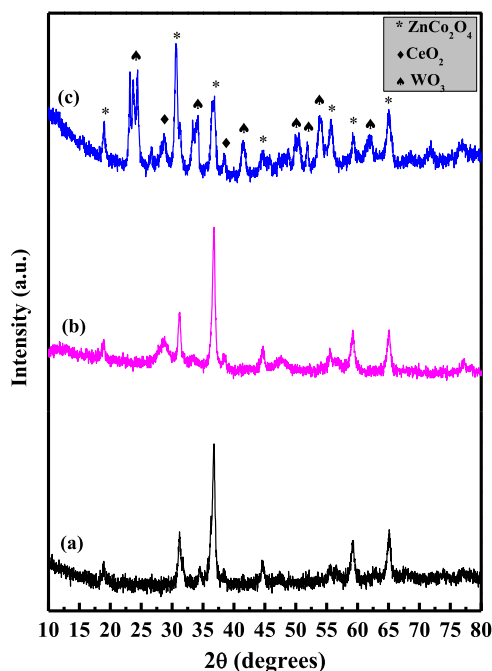


Figure 3. XRD patterns of (a) ZnCo_2O_4 microspheres, (b) $\text{ZnCo}_2\text{O}_4@\text{CeO}_2$ support, and (c) $\text{WO}_3/\text{ZnCo}_2\text{O}_4@\text{CeO}_2$ catalyst.

spheroids display various intense diffraction peaks that appeared at $2\theta = 19.02, 31.20, 36.77, 44.55, 59.17,$ and 65.05° with characteristic planes (600), (711), (751), (808), and (1222), respectively. These diffraction peaks clearly indicate the well-defined cubic crystal system for the ZnCo_2O_4 spheroids as reported elsewhere (JCPDS no. 23–1390).⁴² This shows that the ZnCo_2O_4 microspheres were successfully synthesized by the hydrothermal method. The XRD crystallite size for ZnCo_2O_4 spheres was also calculated and found to be 20.10 nm.

Similarly, CeO_2 -modified ZnCo_2O_4 particles were also analyzed by XRD analysis (Figure 3b). The sample shows two additional diffraction peaks at $2\theta = 28.70$ and 47.87° (JCPDS no. 43-1002) with characteristic planes (111) and (2200) along with the diffraction peaks corresponding to $2\theta = 19.02, 31.20, 36.77, 44.55, 59.17,$ and 65.05° for ZnCo_2O_4 particles. These diffraction peaks clearly indicate the decoration of the crystalline CeO_2 particles on the ZnCo_2O_4 spheroids.^{42–44} Moreover, the diffraction peaks that appeared for CeO_2 are broader as compared with the bare ZnCo_2O_4 , indicating that the shell is composed of tiny-sized CeO_2

nanoparticles.⁴² It is interesting that the structure of the ZnCo_2O_4 spheroids changes from a cubic crystalline system to a triclinic (anorthic) crystal system upon decoration with CeO_2 particles. In addition to the above, the average crystallite size of the $\text{ZnCo}_2\text{O}_4@\text{CeO}_2$ support slightly increased to 21.70 nm (Table S1), showing the successful dispersion of the CeO_2 particles on the ZnCo_2O_4 spheroids. The detail is given here for comparison as reported previously in our manuscript.³⁸

Similarly, the XRD spectrum of the $\text{WO}_3/\text{ZnCo}_2\text{O}_4@\text{CeO}_2$ catalyst shows several diffraction peaks at $2\theta = 23.09, 23.61, 24.32, 26.56, 30.57, 34.12, 38.35, 41.16, 48.80, 49.82, 50.45, 51.77, 54.77, 55.85, 62.22,$ and 77.21° (JCPDS no. 83–0950)⁴⁰ along with the diffraction peaks for the $\text{ZnCo}_2\text{O}_4@\text{CeO}_2$ support. These diffraction peaks with characteristic planes (141), (41–1), (204), (224), (044), (52-3), (613), (552), (646), (931), (844), (933), (1022), (953), (1133), and (1353) indicate the monoclinic WO_3 crystal system distributed on the surface of the $\text{ZnCo}_2\text{O}_4@\text{CeO}_2$ support. The average crystallite size for the catalyst was also estimated and recorded to be 22.71 nm (Table S1). The XRD analysis signifies that WO_3 was successfully decorated on the $\text{ZnCo}_2\text{O}_4@\text{CeO}_2$ support to develop the desired bifunctional heterogeneous catalyst.

3.1.4. Electron Microscopy Analysis (SEM/FESEM). The morphological behaviors of the synthesized catalysts were elaborated by both scanning electron microscopy (SEM) and field emission scanning electron microscopy (FESEM), as given in Figures 4 and S1, respectively.

The SEM analysis of the ZnCo_2O_4 microspheres clearly indicates that the particles are spherical and uniform in size with an almost smooth surface as reported in our previously published article.^{38,45} The SEM particle size for the synthesized spheroids was estimated to be $0.88 \mu\text{m}$. In addition, the FESEM analysis revealed that the ZnCo_2O_4 spheroids are constituted of small granules with an average size of $0.038 \mu\text{m}$ (Figure S1).

Similarly, the SEM results for the $\text{ZnCo}_2\text{O}_4@\text{CeO}_2$ support were also obtained, as shown in Figure 4b. The micrograph clearly indicates that CeO_2 particles were uniformly distributed on the ZnCo_2O_4 spheroids. In addition, the FESEM results reveal that the surface roughness slightly increased when CeO_2 was decorated on the surface of ZnCo_2O_4 particles.

The surface morphology of the WO_3 -modified $\text{ZnCo}_2\text{O}_4@\text{CeO}_2$ catalyst was also investigated by electron microscopy (Figure 4c). The results signified that the original spherical morphology of the $\text{ZnCo}_2\text{O}_4@\text{CeO}_2$ support remained unchanged when WO_3 active species were grafted during the modification process. However, the catalyst surface was more rough as compared to the $\text{ZnCo}_2\text{O}_4@\text{CeO}_2$ support, indicating the growth of WO_3 crystallites on the surface of the $\text{ZnCo}_2\text{O}_4@\text{CeO}_2$ support as supported by the XRD results. The average size of these crystallites was also estimated and found to be $0.092 \mu\text{m}$, as shown in Table S2. The growth of these fiberlike particles on the surface of the support may increase the surface area of the synthesized catalyst and hence improve the accessibility of the reactants to the active sites to produce optimum levulinic acid yield.

3.1.5. Elemental Composition and Dispersion Analysis. The energy-dispersive X-ray and mapping analysis was also performed for the support and WO_3 -modified $\text{ZnCo}_2\text{O}_4@\text{CeO}_2$ catalyst (Figures S2 and S3). The EDX and mapping analysis clearly indicated the successful preparation of the support and the bifunctional heterogeneous catalyst without

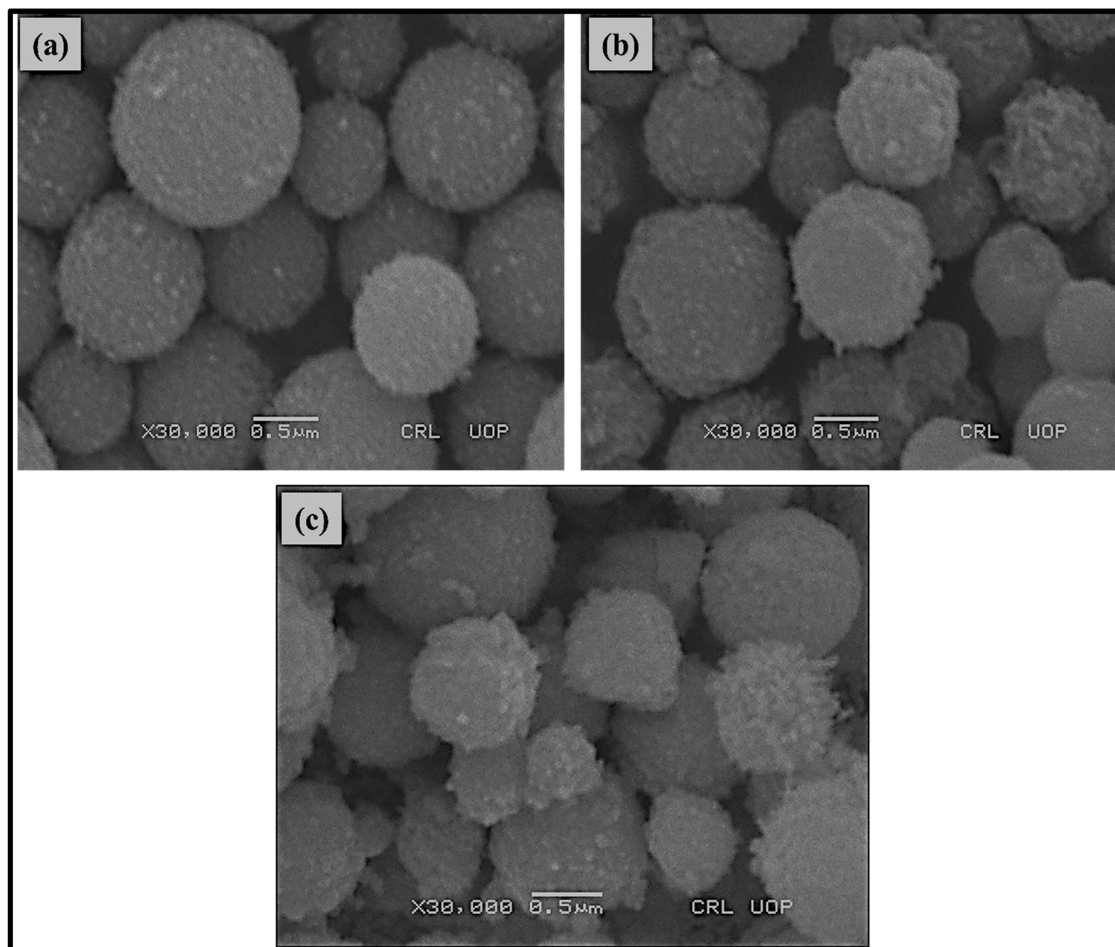


Figure 4. SEM image of (a) ZnCo_2O_4 microspheres, (b) $\text{ZnCo}_2\text{O}_4@ \text{CeO}_2$ catalyst, and (c) $\text{WO}_3/\text{ZnCo}_2\text{O}_4@ \text{CeO}_2$ catalyst.

any elemental loss. Moreover, the energy-dispersive X-ray and mapping analysis show that WO_3 active species are well dispersed on the $\text{ZnCo}_2\text{O}_4@ \text{CeO}_2$ support. The uniform distribution of the active species on the surface of the catalyst will boost the catalytic activity in the desired reaction by providing an optimum number of active sites.

3.1.6. Catalyst Basicity Determination. Carbon dioxide-temperature programmed desorption (TPD) analysis was carried out to study the distribution of basic sites on the surface of the synthesized catalysts (Figure 5). Moreover, the TPD results of the ZnCo_2O_4 spheroids and $\text{ZnCo}_2\text{O}_4@ \text{CeO}_2$ support are also depicted in the same figure for comparison as discussed earlier.³⁸ The TPD results show that the ZnCo_2O_4 spheroid sample possessed basic sites of weak and strong strength at 223 and 800 °C, respectively.⁴⁶ However, the CO_2 -TPD results also show that fewer number of medium basic sites also exist along with the strong and weak basic sites on the catalyst surface.

The distribution of basic sites on the surface of the ZnCo_2O_4 microspheres completely reshuffles upon the modification of ZnCo_2O_4 with CeO_2 particles. It can be observed that the density of the strong basic sites (appeared at 800 °C) decreased when CeO_2 was coated upon ZnCo_2O_4 microspheres, thereby creating relatively less strong basic sites at 362–679 °C. Similarly, the density of weak basic sites in the $\text{ZnCo}_2\text{O}_4@ \text{CeO}_2$ support also increased as compared with bare ZnCo_2O_4 spheroids. Further, the weak basic sites

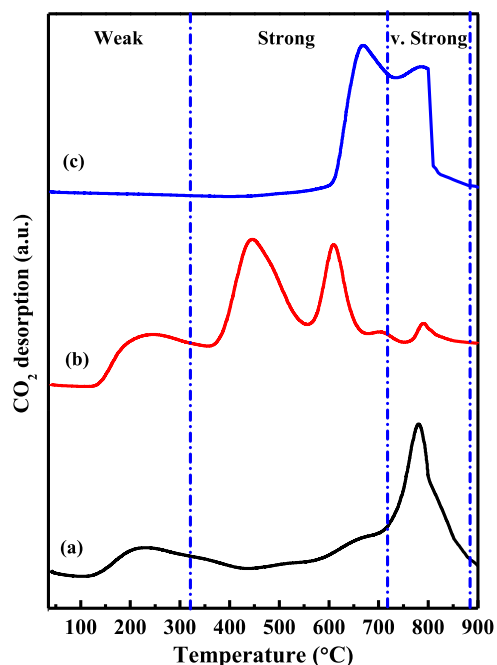


Figure 5. CO_2 -TPD profiles of (a) bare ZnCo_2O_4 spheroids, (b) $\text{ZnCo}_2\text{O}_4@ \text{CeO}_2$ support, and (c) $\text{WO}_3/\text{ZnCo}_2\text{O}_4@ \text{CeO}_2$ catalyst.

appeared at almost the same temperature as was recorded for bare ZnCo_2O_4 spheroids.

The basicity of the $\text{WO}_3/\text{ZnCo}_2\text{O}_4@\text{CeO}_2$ catalyst was also analyzed, as shown in Figure 5c. The results revealed that the $\text{WO}_3/\text{ZnCo}_2\text{O}_4@\text{CeO}_2$ catalyst only possessed basic sites of very strong strength in the temperature range of 600–800 °C. The presence of strong basic sites on the surface of the catalyst can play an important role in the effective interaction with the reactant molecules to produce the desired product in a profitable amount. The details of the basic sites present on the surface of the catalyst are summarized in Table 2.

Table 2. Density of Basic Sites of Bare ZnCo_2O_4 , $\text{ZnCo}_2\text{O}_4@\text{CeO}_2$ Catalyst, and WO_3 -Modified $\text{ZnCo}_2\text{O}_4@\text{CeO}_2$ Catalyst^a

catalyst	density of basic sites (mmol/g)		
	weak	strong	v. strong
ZnCo_2O_4	0.02	n.d.	0.46
$\text{ZnCo}_2\text{O}_4@\text{CeO}_2$	0.04	1.39	0.05
$\text{WO}_3/\text{ZnCo}_2\text{O}_4@\text{CeO}_2$	n.d.	0.67	0.48

^an.d.= not detected.

3.1.7. Catalyst Acidity Determination. Similarly, ammonia-temperature programmed desorption (TPD) analysis was employed to determine the acidity of the synthesized catalysts, and the results are depicted in Figure 6. It can be seen that the

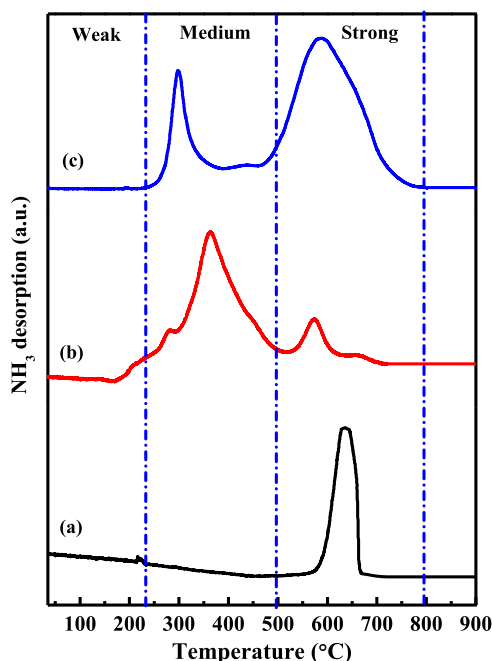


Figure 6. NH_3 -TPD profiles of (a) bare ZnCo_2O_4 microspheres, (b) $\text{ZnCo}_2\text{O}_4@\text{CeO}_2$ catalyst, and (c) $\text{WO}_3/\text{ZnCo}_2\text{O}_4@\text{CeO}_2$ catalyst.

ZnCo_2O_4 bare particles mainly possessed strong acid sites at 640 °C.⁴⁶ In addition, a small peak that appeared at 220 °C is ascribed to the presence of weak acid sites on the surface of the catalyst.

However, the distribution of acid sites significantly changed when the ZnCo_2O_4 particles were decorated with CeO_2 shell, showing a large number of medium acid sites at 360 °C along with some strong acid sites that appeared at 580 °C. The $\text{ZnCo}_2\text{O}_4@\text{CeO}_2$ sample also showed some weak acid sites at 200 °C. The details of the acidity profile of the ZnCo_2O_4

spheroids and $\text{ZnCo}_2\text{O}_4@\text{CeO}_2$ support are discussed here for comparison and have been reported in our previous manuscript.³⁸

On the other hand, NH_3 -TPD analysis of the $\text{WO}_3/\text{ZnCo}_2\text{O}_4@\text{CeO}_2$ catalyst shows a broad desorption peak (Figure 6c) at a temperature maximum of 590 °C, indicating the presence of strong acid sites on the surface of the catalyst. The second relatively small desorption peak that appeared at 300 °C corresponds to the presence of medium acid sites on the surface of the catalyst.

The NH_3 -TPD results further reveal that the grafting of the WO_3 active moieties onto the $\text{ZnCo}_2\text{O}_4@\text{CeO}_2$ support significantly changes the pattern of the acid site strength of the catalyst.

Thus, the presence of both acidic and basic sites of different strengths on the catalyst surface can play a vital role in developing a sustainable levulinic acid production process from waste corncob biomass. The NH_3 -TPD results are further summarized in Table 3.

Table 3. Density of Acid Sites of Bare ZnCo_2O_4 , $\text{ZnCo}_2\text{O}_4@\text{CeO}_2$ Catalyst, and WO_3 -Modified $\text{ZnCo}_2\text{O}_4@\text{CeO}_2$ Catalyst^a

catalyst	density of acid sites (mmol/g)		
	weak	medium	strong
ZnCo_2O_4	0.014	n.d.	0.58
$\text{ZnCo}_2\text{O}_4@\text{CeO}_2$	n.d.	0.83	0.012
$\text{WO}_3/\text{ZnCo}_2\text{O}_4@\text{CeO}_2$	n.d.	0.39	1.93

^an.d.= not detected.

3.2. Catalyst Screening. The catalytic activity of the designed $\text{WO}_3/\text{ZnCo}_2\text{O}_4@\text{CeO}_2$ catalyst with various WO_3 loadings (5, 10, 15 wt %) was evaluated for levulinic acid production from selected biomass under preset reaction conditions (i.e., catalyst dosage of 4 wt %, 180 °C temperature, and 200 min reaction time). It was observed that among the catalysts, WO_3 10 wt %/ $\text{ZnCo}_2\text{O}_4@\text{CeO}_2$ showed the best catalytic activity in levulinic acid production with a yield of 73.73%. The experimental results signify that the catalyst with WO_3 loading of 10 wt % provides sufficient active sites to facilitate the reactants and provide maximum levulinic acid yield.

In view of the above, the reaction parameters were further optimized for the WO_3 10 wt %/ $\text{ZnCo}_2\text{O}_4@\text{CeO}_2$ catalyst to identify economically viable parameters for sustainable levulinic acid production. Moreover, the catalyst was further considered to study the various physicochemical properties by different characterization techniques.

3.2.1. Parametric Optimization. **3.2.1.1. Effect of Catalyst Dosage.** As known, the catalyst dosage has a prominent role in providing sufficient active sites for the given reaction to push the reaction in the forward direction. Therefore, the effect of catalyst loading on LA yield from selected biomass was thoroughly investigated in the range of 2–10 wt % (Figure 7). It was noted that the levulinic acid yield was substantially enhanced with the increase in catalyst loading. This could be related to the fact that as the catalyst amount increases, the number of active sites also increases and hence improves the accessibility of the reactants to the active sites.

However, it was recorded that there was no further increase in the levulinic acid yield under the same conditions upon

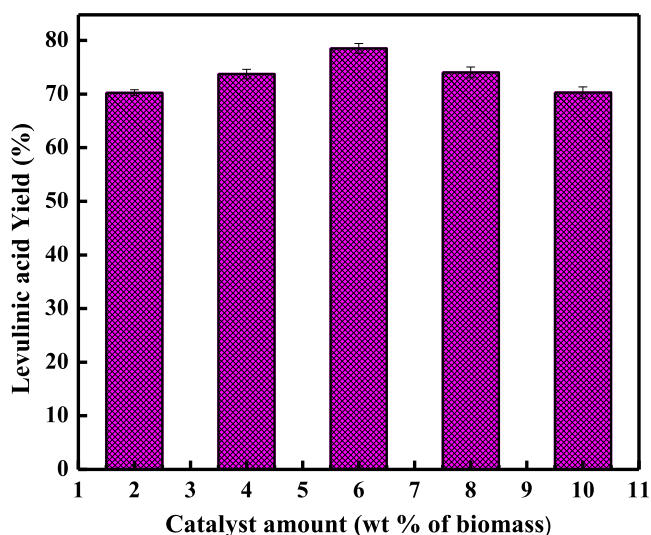


Figure 7. Influence of catalyst dosage on the LA yield (%) from the corncob biomass in the presence of WO_3 10 wt %/ ZnCo_2O_4 @ CeO_2 catalyst at the reaction time of 200 min and a reaction temperature of 180 °C.

increasing the catalyst amount beyond 6 wt %. The decrease in the levulinic acid yield from the selected biomass at a higher catalyst loading could be attributed to various factors:

- (i) The contact between the solid catalyst and reactants may cause the reaction mixture to become thicker when a higher catalyst loading is utilized and creates dispersion problems.⁴⁷
- (ii) The decrease in levulinic acid yield with a higher catalyst loading may be due to humin formation resulting from condensation reactions and aldol addition reactions of 5-HMF.⁴⁸

In view of the above, 6 wt % catalyst dosage was chosen to be the best catalyst amount for the efficient production of levulinic acid from corncob biomass.

3.2.1.2. Effect of Temperature. Temperature has a pivotal role in the thermodynamic behavior of the reaction. Therefore, the effect of temperature must be investigated properly to identify a suitable temperature for the economically viable production of levulinic acid. The influence of reaction temperature on levulinic acid yield from the selected biomass was investigated in the temperature range of 160–210 °C, and the results are enumerated in Figure 8.

It can be seen that levulinic acid yield sufficiently improved as the reaction temperature was increased. The higher reaction temperature accelerates the kinetic energy of the reaction molecules, which then results in a greater number of effective collisions to overcome the miscibility and mass transfer limitations.⁴⁹ This clearly indicates that the biomass conversion into levulinic acid is endothermic in nature and therefore favors the high temperature for efficient conversion. This further justified that the glucose conversion to levulinic acid completes at nearly 180 °C.⁵⁰ Moreover, the electron transfer ability may increase at high temperatures, resulting in an increase in the reaction rate.⁵¹ The maximum levulinic acid yield of 78.49% was achieved at a reaction temperature of 180 °C while keeping the other parameters constant.

However, the levulinic acid yield decreased when the reaction temperature was further increased above 180 °C, i.e., the optimum reaction temperature. The decrease of

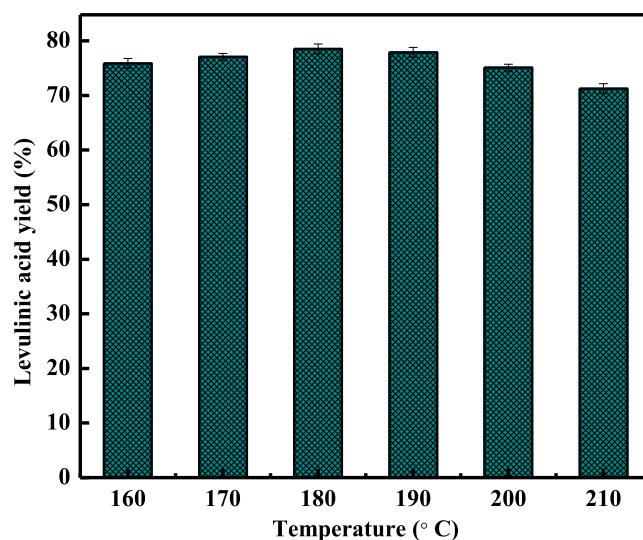


Figure 8. Influence of temperature on LA yield (%) from corncob biomass in the presence of WO_3 10 wt %/ ZnCo_2O_4 @ CeO_2 catalyst at 200 min reaction time with 6 wt % catalyst dosage.

levulinic acid yield with an increase in temperature may be attributed to many reasons.

- (i) Water-soluble and insoluble humins may form at elevated temperatures, hindering the yield of levulinic acid.^{48,52,53}
- (ii) Undesired side reactions may accelerate under a high reaction temperature, resulting in reduced yield of levulinic acid.⁵⁴
- (iii) Formation of humic polymers is the main competing pathway in the conversion of HMF to levulinic acid, which increases at higher reaction temperatures.⁵⁵

Therefore, in this study, the reaction temperature of 180 °C was chosen for the efficient conversion of corncob biomass waste into levulinic acid.

3.2.1.3. Effect of Reaction Time. The reaction time is another important parameter that greatly influences the LA production from biomass as the reactants need sufficient interaction time with the active sites to convert into the final product. The reaction time was also evaluated in the range of 180–220 min to minimize the overall cost of the process (Figure 9).

It was significantly observed that the levulinic acid yield increased as the reaction time was increased while keeping the other experimental parameters constant, i.e., 6 wt % catalyst dosage and 180 °C reaction temperature. The reaction provided the highest yield of 78.49% levulinic acid at a reaction time of 200 min. This indicates that 200 min provides a sufficient time span for the reactants to interact efficiently and convert into the final products.

However, a slight decrease in the LA yield was noticed when the reaction was performed for more than 200 min. This decrease in the levulinic acid yield could be due to the fact that dehydrated products may be unstable and undergo decomposition when exposed to higher temperatures for a longer time. Moreover, side reactions may be accelerated when the hydrolysis of biomass is carried out for a prolonged time, resulting in char and humin formation.^{48,53} In addition, degradation of levulinic acid takes place when the reaction is prolonged, causing a decrease in the yield of levulinic acid.⁵⁰

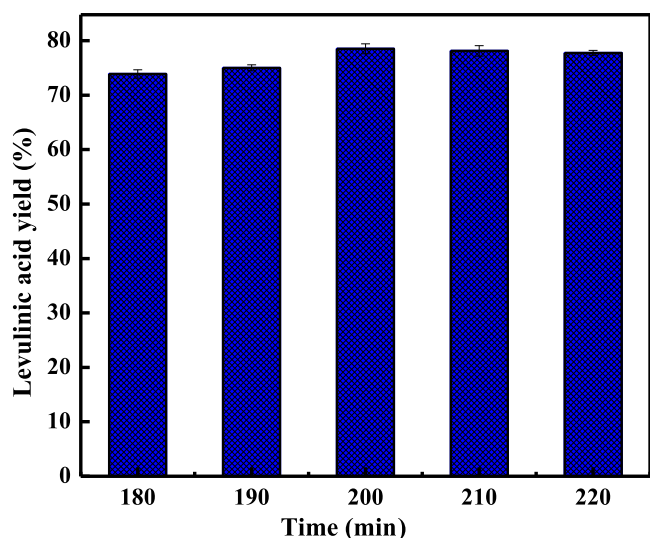


Figure 9. Influence of time on LA yield (%) from selected biomass in the presence of WO_3 10 wt %/ ZnCo_2O_4 @ CeO_2 catalyst at 6 wt % catalyst dosage and temperature of 180°C .

Therefore, a reaction time of 200 min was selected as the optimal reaction time for the conversion of corncob biomass into levulinic acid using WO_3 10 wt %/ ZnCo_2O_4 @ CeO_2 catalyst.

3.3. Product Analysis. **3.3.1. Gas Chromatography Analysis.** The purified organic product was analyzed for LA by GC technique, as shown in Figure 10. The GC chromatogram showed the presence of two major products in the sample collected from the reaction mixture. The components were identified by comparing with the GC libraries (NL: 5.25 E8 TIC MS) and literature. The peak that appeared at 1.69 retention time shows the presence of furfural in the organic sample collected from the reaction mixture. The second peak with a retention time of 3.57 is mainly assigned to LA formed during the hydrolysis of C6 sugars of the biomass. The GC results signify that the corncob biomass was converted efficiently into LA in the presence of WO_3 10 wt %/ ZnCo_2O_4 @ CeO_2 catalyst. Thus, the good

performance of the catalyst for LA production from biomass will open new avenues for researchers to develop a robust catalyst for the biochemical production process.

3.4. Catalyst Reusability. The reusability study of the catalyst is essential for the determination of the economic viability in large-scale production. Therefore, the recyclability of the WO_3 10 wt %/ ZnCo_2O_4 @ CeO_2 catalyst was investigated for LA production from selected biomass at optimal reaction conditions, as shown in Figure 11.

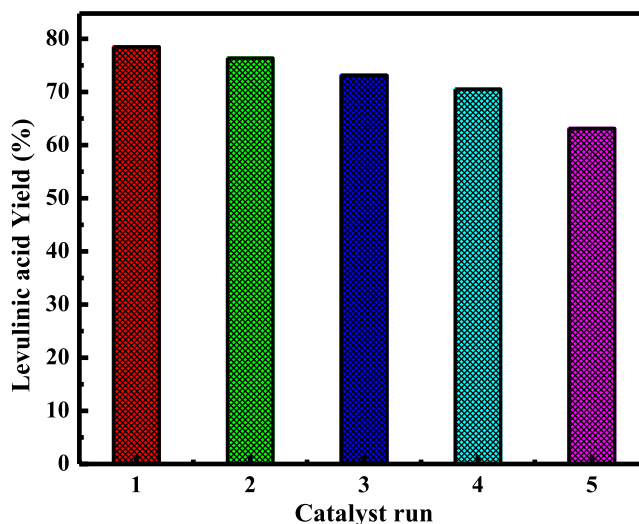


Figure 11. Reusability study of the WO_3 10 wt %/ ZnCo_2O_4 @ CeO_2 catalyst for LA production from selected biomass at optimal experimental conditions.

After each reaction run, the reaction mixture was filtered and the catalyst was recovered carefully. The recovered catalyst was first dried and then calcined at 400°C to wipe out the undesired substances from the catalyst surface and then tested in the new reaction for LA.

The reusability results indicated that the designed catalyst sustained sufficient reusability up to four reuses, showing that the catalyst is chemically and thermally sound. However, the

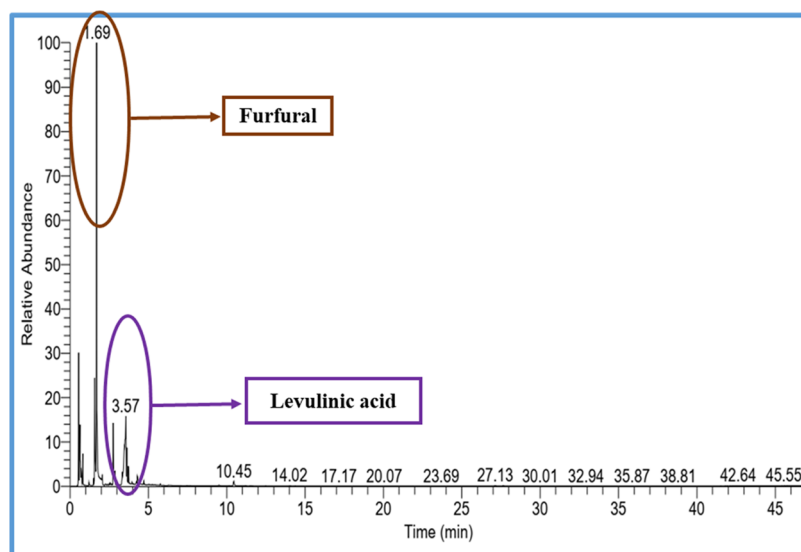
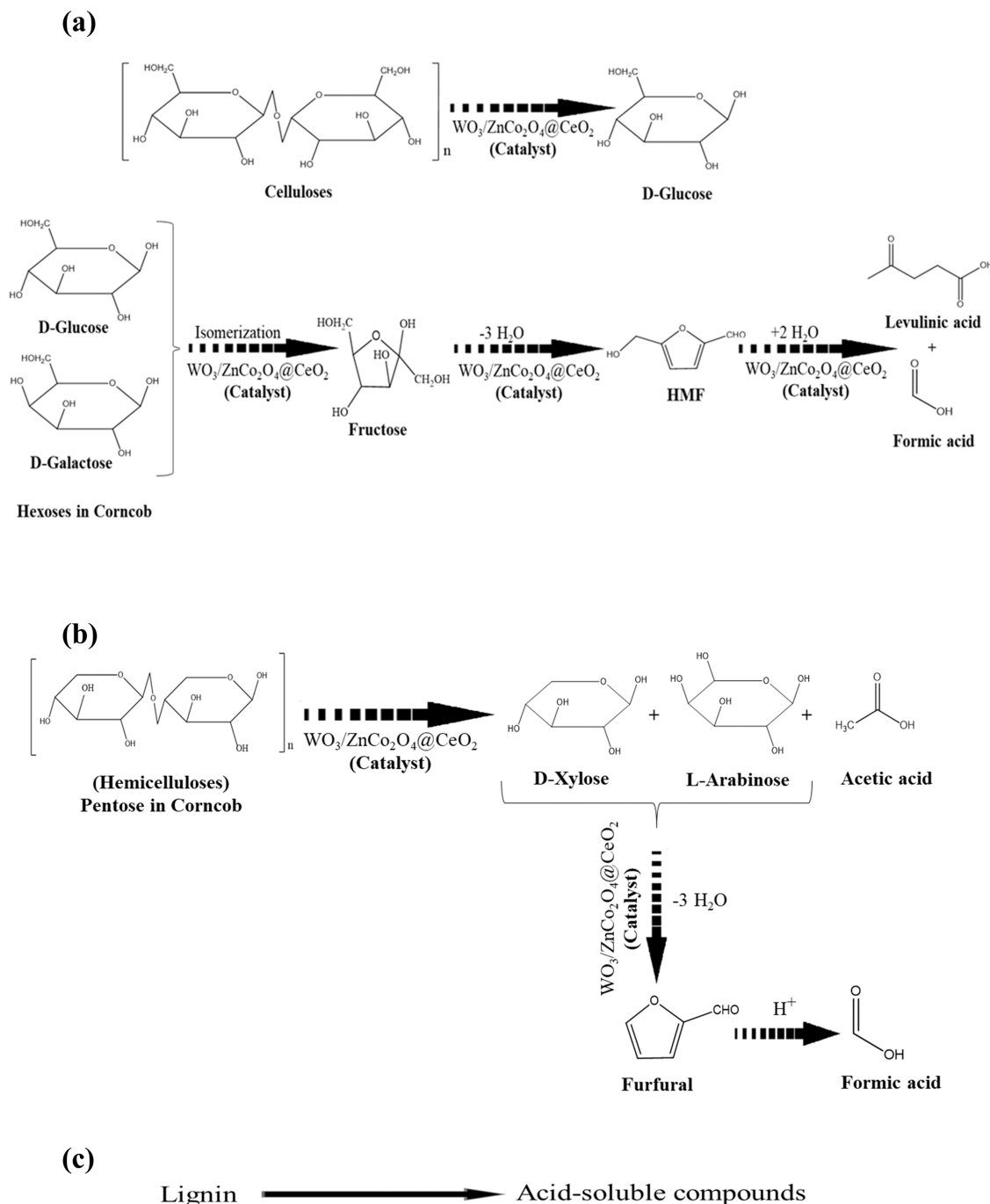


Figure 10. GC spectra of the product obtained from the hydrolysis of corncob biomass using the WO_3 10 wt %/ ZnCo_2O_4 @ CeO_2 catalyst.

Scheme 1. Schematic Pathway for Catalytic Conversion of Biomass into Different Products



catalytic activity slightly decreased when used more than four times for levulinic acid production. This may be due to the coke deposition and unburned substances trapped within the pores of the catalyst. But the catalytic activity is regenerated when calcined at high temperatures.

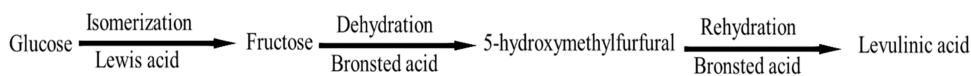
Moreover, the heterogeneity behavior of the catalyst was studied using a hot filtration test under the optimized reaction conditions. For this, the reaction was stopped after its 50% completion and the catalyst was separated from the reaction mixture. The reaction mixture was further proceeded without a catalyst under the same reaction conditions. After the reaction completion, it was noted that there was no further increase in the conversion, signifying that no active species have leaked out during the reaction. Similarly, the obtained product from

each run was also analyzed by atomic absorption spectroscopy (AAS), wherein no trace elements were recorded. This confirms that the active moieties are strongly bridged to the support surface, which helps to overcome the leaching of the active species from the surface.

In summary, the designed catalyst has tremendous potential toward an eco-friendly and sustainable approach for the production of valued chemicals from waste biomass in the near future.

3.5. Proposed Reaction Pathway. The cellulosic part of the biomass can be converted into valued products via catalytic hydrolysis involving different reactions such as cellulose depolymerization, glucose isomerization, fructose dehydration, and hydroxymethylfurfural rehydration. The detailed mecha-

Scheme 2. Schematic Presentation of Levulinic Acid Production from Glucose



nism for the conversion of various components of the biomass into levulinic acid is given in the proposed Scheme 1.

In the depolymerization step, acid hydrolysis conversion of cellulose to glucose takes place on the Bronsted acid sites of the catalyst. Likewise, the isomerization reaction is catalyzed by the Lewis acid sites of the catalyst, wherein glucose is isomerized to fructose.⁵⁶ The dehydration reaction, in which fructose is converted to 5-HMF, and the rehydration reaction, where furfural is converted into LA, are both catalyzed by the Bronsted acid sites on the surface of the catalyst.

Thus, the simultaneous cellulose hydrolysis and glucose isomerization on the Bronsted and Lewis acid sites, respectively, enhance the overall catalyst efficiency to produce the highest LA yield.^{9,57–59}

In this study, the $\text{WO}_3/\text{ZnCo}_2\text{O}_4@\text{CeO}_2$ catalyst was employed to convert the waste corncob biomass into LA. The designed catalyst possesses the synergistic characteristics of Bronsted and Lewis acid sites, which enlighten its potency for efficient LA production from waste biomass. The general reaction for glucose conversion into levulinic acid is also simplified by the equation given in Scheme 2 as reported elsewhere.⁹

The hemicellulosic part of the biomass is mainly comprised of C_5 sugars such as xylose, arabinose, and mannose along with some C_6 sugars such as galactose. The C_6 sugars dehydrate during the acid hydrolysis process and produce 5-HMF, which is then converted into LA upon rehydration.

On the other hand, the C_5 sugars are converted into D-xylose, L-arabinose, and acetic acid upon the acid hydrolysis and later convert to furfural on dehydration. It has been reported that the furfural is very difficult to convert into LA at the normal experimental conditions as enumerated in the proposed Scheme 1.⁶⁰

Generally, furfural conversion into LA involves very complex reactions like (i) the conversion of furfural to furfuryl alcohol through hydrogenation (ii) and the conversion of furfuryl alcohol later into levulinic acid under an acidic medium.⁵⁹ Similarly, the furfural containing aromatic furan ring is first modified with a hydroxyl group through an electrophilic substitution reaction, which then changes into hydroxymethylfurfural through electrophilic reagents media and finally changes into levulinic acid.⁵⁹

The lignin constituent of the biomass (resin like polymer) can be converted into various acid-soluble lignin-derived compounds upon acid hydrolysis.⁶¹

4. CONCLUSIONS

In this study, a bifunctional heterogeneous catalyst was successfully designed by grafting WO_3 active species onto the $\text{ZnCo}_2\text{O}_4@\text{CeO}_2$ support surface for economical viable production of LA from selected corncob biomass. Various analytical techniques were employed to characterize the synthesized catalyst and gain insight into the crucial physicochemical properties.

It was explored that the WO_3 10 wt %/ $\text{ZnCo}_2\text{O}_4@\text{CeO}_2$ catalyst showed enhanced catalytic activity at the optimal experimental conditions such as catalyst dosage of 6 wt %, reaction temperature of 180 °C, and reaction time of 200 min,

providing a maximum yield of 78.49% for levulinic acid. The good performance of the designed catalyst is assigned to the acid–base synergistic behavior of the catalyst.

Moreover, the sustainability results clearly indicated that the WO_3 10 wt %/ $\text{ZnCo}_2\text{O}_4@\text{CeO}_2$ catalyst retains sufficient reusability up to four reuses for levulinic acid production from corncob biomass with negligible loss in the catalyst performance.

It is recommended to investigate the catalytic performance of the synthesized catalyst for levulinic acid production in a high-pressure reactor under an inert atmosphere using an appropriate cosolvent to develop an environmentally friendly approach for profitable and sustainable levulinic acid production from corncob biomass.

The overall study shows that WO_3 10 wt %/ $\text{ZnCo}_2\text{O}_4@\text{CeO}_2$ has promising potency toward sustainable and environmentally benign bioindustries based on waste biomass.

■ ASSOCIATED CONTENT

Supporting Information

The Supporting Information is available free of charge at <https://pubs.acs.org/doi/10.1021/acsomega.2c04545>.

FESEM image of ZnCo_2O_4 spheroids, $\text{ZnCo}_2\text{O}_4@\text{CeO}_2$ support, and WO_3 -modified $\text{ZnCo}_2\text{O}_4@\text{CeO}_2$ catalyst (Figure S1); elemental dispersion analysis of ZnCo_2O_4 spheroids, $\text{ZnCo}_2\text{O}_4@\text{CeO}_2$ support, and WO_3 -modified $\text{ZnCo}_2\text{O}_4@\text{CeO}_2$ catalyst (Figure S2); mapping analysis of WO_3 -modified $\text{ZnCo}_2\text{O}_4@\text{CeO}_2$ catalyst (Figure S3); crystal size of ZnCo_2O_4 spheroids, $\text{ZnCo}_2\text{O}_4@\text{CeO}_2$ support, and WO_3 -modified $\text{ZnCo}_2\text{O}_4@\text{CeO}_2$ catalyst (Table S1); and average sizes of ZnCo_2O_4 spheroids, $\text{ZnCo}_2\text{O}_4@\text{CeO}_2$ support, and WO_3 -modified $\text{ZnCo}_2\text{O}_4@\text{CeO}_2$ catalyst (Table S2) (PDF)

■ AUTHOR INFORMATION

Corresponding Authors

Fouzia Perveen – National Centre of Excellence in Physical Chemistry, University of Peshawar, Peshawar 25120 Khyber Pakhtunkhwa, Pakistan; orcid.org/0000-0002-1748-6284; Email: fouziaperveen82@yahoo.com

Muhammad Farooq – National Centre of Excellence in Physical Chemistry, University of Peshawar, Peshawar 25120 Khyber Pakhtunkhwa, Pakistan; Email: farooq_khann@yahoo.com

Authors

Anita Ramli – Department of Fundamental and Applied Sciences, Universiti Teknologi PETRONAS, Tronoh 31750, Malaysia

Abdul Naeem – National Centre of Excellence in Physical Chemistry, University of Peshawar, Peshawar 25120 Khyber Pakhtunkhwa, Pakistan

Ihtisham Wali Khan – National Centre of Excellence in Physical Chemistry, University of Peshawar, Peshawar 25120 Khyber Pakhtunkhwa, Pakistan

Tooba Saeed – National Centre of Excellence in Physical Chemistry, University of Peshawar, Peshawar 25120 Khyber Pakhtunkhwa, Pakistan

Jehangeer Khan – National Centre of Excellence in Physical Chemistry, University of Peshawar, Peshawar 25120 Khyber Pakhtunkhwa, Pakistan

Complete contact information is available at:
<https://pubs.acs.org/10.1021/acsomega.2c04545>

Funding

The authors declare that no funds, grants, or other support were received during the preparation of this manuscript.

Notes

The authors declare no competing financial interest.

ACKNOWLEDGMENTS

The authors acknowledge National Centre of Excellence in Physical Chemistry, University of Peshawar, Pakistan, and Universiti Teknologi PETRONAS, Malaysia to complete research work.

REFERENCES

- (1) Khan, I. W.; Naeem, A.; Farooq, M.; Mahmood, T.; Ahmad, B.; Hamayun, M.; Ahmad, Z.; Saeed, T. Catalytic conversion of spent frying oil into biodiesel over raw and 12-tungsto-phosphoric acid modified clay. *Renewable Energy*. **2020**, *155*, 181–188.
- (2) Wang, B.; Cong, H.; Li, X.; Li, H.; Gao, X. Selective and efficient separation of biomass hydrolysate levulinic acid and formic acid from aqueous solution. *Chem. Eng. Res. Des.* **2022**, *181*, 266–277.
- (3) Jeong, G.-T.; Kim, S.-K. Platform chemicals production from lipid-extracted *Chlorella vulgaris* through an eco-friendly catalyst. *Korean J. Chem. Eng.* **2021**, *38*, 997–1005.
- (4) Zong, R.; Li, H.; Ding, W.; Huang, H. Highly dispersed Pd on zeolite/carbon nanocomposites for selective hydrodeoxygenation of biomass-derived molecules under mild conditions. *ACS Sustainable Chem. Eng.* **2021**, *9*, 9891–9902.
- (5) Xu, S.; Yu, D.; Ye, T.; Tian, P. Catalytic transfer hydrogenation of levulinic acid to γ -valerolactone over a bifunctional tin catalyst. *RSC Adv.* **2017**, *7*, 1026–1031.
- (6) Wei, H.; Wang, Z.; Li, H. Sustainable biomass hydrodeoxygenation in biphasic systems. *Green Chem.* **2022**, *24*, 1930–1950.
- (7) Hendriks, A.; Zeeman, G. Pretreatments to enhance the digestibility of lignocellulosic biomass. *Bioresour. Technol.* **2009**, *100*, 10–18.
- (8) Pattanaik, F.; Tripathi, S.; Patra, B. R.; Nanda, S.; Kumar, V.; Dalai, A. K.; Naik, S. Catalytic conversion of lignocellulosic polysaccharides to commodity biochemicals: a review. *Environ. Chem. Lett.* **2021**, *19*, 4119–4136.
- (9) Qu, H.; Liu, B.; Gao, G.; Ma, Y.; Zhou, Y.; Zhou, H.; Li, L.; Li, Y.; Liu, S. Metal-organic framework containing Brønsted acidity and Lewis acidity for efficient conversion glucose to levulinic acid. *Fuel Process. Technol.* **2019**, *193*, 1–6.
- (10) Alonso, D. M.; Bond, J. Q.; Dumesic, J. A. Catalytic conversion of biomass to biofuels. *Green Chem.* **2010**, *12*, 1493–1513.
- (11) Mikola, M.; Ahola, J.; Tanskanen, J. Production of levulinic acid from glucose in sulfolane/water mixtures. *Chem. Eng. Res. Des.* **2019**, *148*, 291–297.
- (12) Loow, Y.-L.; Wu, T. Y.; Tan, K. A.; Lim, Y. S.; Siow, L. F.; Md Jahim, J.; Mohammad, A. W.; Teoh, W. H. Recent advances in the application of inorganic salt pretreatment for transforming lignocellulosic biomass into reducing sugars. *J. Agric. Food Chem.* **2015**, *63*, 8349–8363.
- (13) Saleem, M.; Rustam, M.; Naqvi, H. J.; Jabeen, S.; Akhtar, A. Synthesis of precipitated silica from corn cob by using organic acids. *Sci. Int.* **2014**, 265–269.
- (14) Osman, A. I.; Fawzy, S.; Farghali, M.; El-Azazy, M.; Elgarahy, A. M.; Fahim, R. A.; Maksoud, M.; Ajlan, A. A.; Yousry, M.; Saleem, Y.; Rooney, D. W. Biochar for agronomy, animal farming, anaerobic digestion, composting, water treatment, soil remediation, construction, energy storage, and carbon sequestration: a review. *Environ. Chem. Lett.* **2022**, *20*, 2385–2485.
- (15) Barla, M. K.; Velagala, R. R.; Minpoor, S.; Madduluri, V. R.; Srinivasu, P. Biomass derived efficient conversion of levulinic acid for sustainable production of γ -valerolactone over cobalt based catalyst. *J. Hazard. Mater.* **2021**, *405*, No. 123335.
- (16) Osman, A. I.; Mehta, N.; Elgarahy, A. M.; Al-Hinai, A.; Al-Muhtaseb, A. a. H.; Rooney, D. W. Conversion of biomass to biofuels and life cycle assessment: a review. *Environ. Chem. Lett.* **2021**, *19*, 4075–4118.
- (17) Cha, J. S.; Um, B. H. Levulinic acid production through two-step acidic and thermal treatment of food waste using dilute hydrochloric acid. *Korean J. Chem. Eng.* **2020**, *37*, 1149–1156.
- (18) Hijazi, A.; Khalaf, N.; Kwapinski, W.; Leahy, J. Catalytic valorisation of biomass levulinic acid into gamma valerolactone using formic acid as a H₂ donor: a critical review. *RSC Adv.* **2022**, *12*, 13673–13694.
- (19) Pyo, S.-H.; Glaser, S. J.; Rehnberg, N.; Hatti-Kaul, R. Clean production of levulinic acid from fructose and glucose in salt water by heterogeneous catalytic dehydration. *ACS Omega*. **2020**, *5*, 14275–14282.
- (20) Liu, S.; Cheng, X.; Sun, S.; Chen, Y.; Bian, B.; Liu, Y.; Tong, L.; Yu, H.; Ni, Y.; Yu, S. High-Yield and High-Efficiency Conversion of HMF to Levulinic Acid in a Green and Facile Catalytic Process by a Dual-Function Brønsted-Lewis Acid HScCl₄ Catalyst. *ACS Omega* **2021**, *6*, 15940–15947.
- (21) Ramli, N. A. S.; Amin, N. A. S. Kinetic study of glucose conversion to levulinic acid over Fe/HY zeolite catalyst. *Chem. Eng. J.* **2016**, *283*, 150–159.
- (22) Fang, Z.; Qi, X. *Production of Platform Chemicals from Sustainable Resources*; Springer, 2017.
- (23) Guzmán, I.; Heras, A.; Guemez, M.; Iriondo, A.; Cambra, J. F.; Requies, J. Levulinic acid production using solid-acid catalysis. *Ind. Eng. Chem. Res.* **2016**, *55*, 5139–5144.
- (24) Mamman, A. S.; Lee, J. M.; Kim, Y. C.; Hwang, I. T.; Park, N. J.; Hwang, Y. K.; Chang, J. S.; Hwang, J. S. Furfural: Hemicellulose/xylooligomer-derived biochemical. *Biofuels, Bioprod. Biorefin.* **2008**, *2*, 438–454.
- (25) Zhang, W.; Wang, Z.; Huang, J.; Jiang, Y. Zirconia-based solid acid catalysts for biomass conversion. *Energy Fuels* **2021**, *35*, 9209–9227.
- (26) Li, M.; Chen, J.; Li, L.; Ye, C.; Lin, X.; Qiu, T. Novel multi-SO₃H functionalized ionic liquids as highly efficient catalyst for synthesis of biodiesel. *Green Energy Environ.* **2021**, *6*, 271–282.
- (27) Islam, M. G. U.; Jan, M. T.; Farooq, M.; Naeem, A.; Khan, I. W.; Khattak, H. U. Biodiesel production from wild olive oil using TPA decorated Cr–Al acid heterogeneous catalyst. *Chem. Eng. Res. Des.* **2022**, *178*, 540–549.
- (28) Mohebbi, S.; Rostamizadeh, M.; Kahforoushan, D. Effect of molybdenum promoter on performance of high silica MoO₃/B-ZSM-5 nanocatalyst in biodiesel production. *Fuel* **2020**, *266*, No. 117063.
- (29) Ketzner, F.; Celante, D.; de Castilhos, F. Catalytic performance and ultrasonic-assisted impregnation effects on WO₃/USY zeolites in esterification of oleic acid with methyl acetate. *Microporous Mesoporous Mater.* **2020**, *291*, No. 109704.
- (30) Aravindraj, K.; Mohana Roopan, S. WO₃-based materials as heterogeneous catalysts for diverse organic transformations: a mini-review. *Synth. Commun.* **2022**, *52*, 1457–1476.
- (31) Selvaraju, G.; Bakar, N. K. A. Production of a new industrially viable green-activated carbon from Artocarpus integer fruit processing waste and evaluation of its chemical, morphological and adsorption properties. *J. Cleaner Prod.* **2017**, *141*, 989–999.
- (32) Osman, A. I.; Abu-Dahrieh, J. K.; Abdelkader, A.; Hassan, N. M.; Laffir, F.; McLaren, M.; Rooney, D. Silver-modified η -Al₂O₃ catalyst for DME production. *J. Phys. Chem. C* **2017**, *121*, 25018–25032.
- (33) Qing, Q.; Guo, Q.; Zhou, L.; Wan, Y.; Xu, Y.; Ji, H.; Gao, X.; Zhang, Y. Catalytic conversion of corncob and corncob pretreatment

hydrolysate to furfural in a biphasic system with addition of sodium chloride. *Bioresour. Technol.* **2017**, *226*, 247–254.

(34) Tiong, Y. W.; Yap, C. L.; Gan, S.; Yap, W. S. P. Kinetic and thermodynamic studies of oil palm mesocarp fiber cellulose conversion to levulinic acid and upgrading to ethyl levulinate via indium trichloride-ionic liquids. *Renewable Energy* **2020**, *146*, 932–943.

(35) Alonso, D. M.; Wettstein, S. G.; Bond, J. Q.; Root, T. W.; Dumesic, J. A. Production of biofuels from cellulose and corn stover using alkylphenol solvents. *ChemSusChem* **2011**, *4*, 1078–1081.

(36) Alves, A.; Berutti, F.; Clemens, F.; Graule, T.; Bergmann, C. The effect of heat treatment temperature on CeO₂ and Y₂O₃ doped CeO₂ electrospun fibers. *Rev. Adv. Mater. Sci.* **2009**, *21*, 200–204.

(37) Miguel-García, I.; Parres-Escápez, S.; Lozano-Castelló, D.; Bueno-López, A. H₂ assisted decomposition of cerium nitrate to ceria with enhanced catalytic properties. *Catal. Commun.* **2010**, *11*, 848–852.

(38) Perveen, F.; Farooq, M.; Naeem, A.; Humayun, M.; Saeed, T.; Khan, I. W.; Abid, G. Catalytic conversion of agricultural waste biomass into valued chemical using bifunctional heterogeneous catalyst: A sustainable approach. *Catal. Commun.* **2022**, *171*, No. 106516.

(39) Hunyadi, D.; Sajó, I.; Szilágyi, I. M. Structure and thermal decomposition of ammonium metatungstate. *J. Therm. Anal. Calorim.* **2014**, *116*, 329–337.

(40) Gui, Y.; Dong, F.; Zhang, Y.; Zhang, Y.; Tian, J. Preparation and gas sensitivity of WO₃ hollow microspheres and SnO₂ doped heterojunction sensors. *Mater. Sci. Semicond. Process.* **2013**, *16*, 1531–1537.

(41) Yang, X.-L.; Dai, W.-L.; Guo, C.; Chen, H.; Cao, Y.; Li, H.; He, H.; Fan, K. Synthesis of novel core-shell structured WO₃/TiO₂ spheroids and its application in the catalytic oxidation of cyclopentene to glutaraldehyde by aqueous H₂O₂. *J. Catal.* **2005**, *234*, 438–450.

(42) Wang, F.; Wang, X.; Liu, D.; Zhen, J.; Li, J.; Wang, Y.; Zhang, H. High-performance ZnCo₂O₄@CeO₂ core@shell microspheres for catalytic CO oxidation. *ACS Appl. Mater.* **2014**, *6*, 22216–22223.

(43) Damyanova, S.; Bueno, J. Effect of CeO₂ loading on the surface and catalytic behaviors of CeO₂-Al₂O₃-supported Pt catalysts. *Appl. Catal., A* **2003**, *253*, 135–150.

(44) Profeti, L. P.; Ticianelli, E. A.; Assaf, E. M. Production of hydrogen via steam reforming of biofuels on Ni/CeO₂-Al₂O₃ catalysts promoted by noble metals. *Int. J. Hydrogen Energy* **2009**, *34*, 5049–5060.

(45) Hu, L.; Qu, B.; Li, C.; Chen, Y.; Mei, L.; Lei, D.; Chen, L.; Li, Q.; Wang, T. Facile synthesis of uniform mesoporous ZnCo₂O₄ microspheres as a high-performance anode material for Li-ion batteries. *J. Mater. Chem. A* **2013**, *1*, 5596–5602.

(46) Mujmule, R. B.; Jadhav, H. S.; Kim, H. Synergetic effect of ZnCo₂O₄/inorganic salt as a sustainable catalyst system for CO₂ utilization. *J. Environ. Manage.* **2021**, *298*, No. 113433.

(47) Yu, Q.; Wu, X.; Tang, C.; Qi, L.; Liu, B.; Gao, F.; Sun, K.; Dong, L.; Chen, Y. Textural, structural, and morphological characterizations and catalytic activity of nanosized CeO₂-MO_x (M = Mg²⁺, Al³⁺, Si⁴⁺) mixed oxides for CO oxidation. *J. Colloid Interface Sci.* **2011**, *354*, 341–352.

(48) Joshi, S. S.; Zodge, A. D.; Pandare, K. V.; Kulkarni, B. D. Efficient conversion of cellulose to levulinic acid by hydrothermal treatment using zirconium dioxide as a recyclable solid acid catalyst. *Ind. Eng. Chem. Res.* **2014**, *53*, 18796–18805.

(49) Hoque, M. E.; Singh, A.; Chuan, Y. L. Biodiesel from low cost feedstocks: The effects of process parameters on the biodiesel yield. *Biomass Bioenergy* **2011**, *35*, 1582–1587.

(50) Liu, Y.; Li, H.; He, J.; Zhao, W.; Yang, T.; Yang, S. Catalytic conversion of carbohydrates to levulinic acid with mesoporous niobium-containing oxides. *Catal. Commun.* **2017**, *93*, 20–24.

(51) Ramli, N. A. S.; Amin, N. A. S. Fe/HY zeolite as an effective catalyst for levulinic acid production from glucose: characterization and catalytic performance. *Appl. Catal., B* **2015**, *163*, 487–498.

(52) Weingarten, R.; Conner, W. C.; Huber, G. W. Production of levulinic acid from cellulose by hydrothermal decomposition combined with aqueous phase dehydration with a solid acid catalyst. *Energy Environ. Sci.* **2012**, *5*, 7559–7574.

(53) Patil, S. K. R.; Lund, C. R. Formation and growth of humins via aldol addition and condensation during acid-catalyzed conversion of 5-hydroxymethylfurfural. *Energy Fuels* **2011**, *25*, 4745–4755.

(54) Wei, W.; Yang, H.; Wu, S. Efficient conversion of carbohydrates into levulinic acid over chromium modified niobium phosphate catalyst. *Fuel* **2019**, *256*, No. 115940.

(55) Girisuta, B.; Janssen, L.; Heeres, H. A kinetic study on the decomposition of 5-hydroxymethylfurfural into levulinic acid. *Green Chem.* **2006**, *8*, 701–709.

(56) Khan, A. S.; Man, Z.; Bustam, M. A.; Kait, C. F.; Nasrullah, A.; Ullah, Z.; Sarwono, A.; Ahamd, P.; Muhammad, N. Dicationic ionic liquids as sustainable approach for direct conversion of cellulose to levulinic acid. *J. Cleaner Prod.* **2018**, *170*, 591–600.

(57) Wei, W.; Wu, S. Experimental and kinetic study of glucose conversion to levulinic acid in aqueous medium over Cr/HZSM-5 catalyst. *Fuel* **2018**, *225*, 311–321.

(58) Yu, F.; Thomas, J.; Smet, M.; Dehaen, W.; Sels, B. F. Molecular design of sulfonated hyperbranched poly(arylene oxindole)s for efficient cellulose conversion to levulinic acid. *Green Chem.* **2016**, *18*, 1694–1705.

(59) Feng, J.; Tong, L.; Xu, Y.; Jiang, J.; Hse, C.; Yang, Z.; Pan, H. Synchronous conversion of lignocellulosic polysaccharides to levulinic acid with synergic bifunctional catalysts in a biphasic cosolvent system. *Ind. Crops. Prod.* **2020**, *145*, No. 112084.

(60) Ren, J.; Wang, W.; Yan, Y.; Deng, A.; Chen, Q.; Zhao, L. Microwave-assisted hydrothermal treatment of corncob using tin (IV) chloride as catalyst for furfural production. *Cellulose* **2016**, *23*, 1649–1661.

(61) Liu, L.; Li, Z.; Hou, W.; Shen, H. Direct conversion of lignocellulose to levulinic acid catalyzed by ionic liquid. *Carbohydr. Polym.* **2018**, *181*, 778–784.